Materials Science and Engineering C 31 (2011) 545–552

Contents lists available at ScienceDirect

Materials Science and Engineering C

journal homepage: www.elsevier.com/locate/msec

Morphologic and nanomechanical characterization of bone tissue growth around bioactive sol–gel coatings containing wollastonite particles applied on stainless steel implants

Josefina Ballarre [a,*], Rocío Seltzer [b], Emigdio Mendoza [c], Juan Carlos Orellano [d], Yiu-Wing Mai [b], Claudia García [c], Silvia M. Ceré [a]

[a] INTEMA, Universidad Nacional de Mar del Plata, Juan B Justo 4302, B7608FDQ Mar del Plata, Buenos Aires, Argentina
[b] Center for Advanced Materials Technology (CAMT), School of Aerospace, Mechanical and Mechatronic Engineering J07, University of Sydney, Sydney, Australia
[c] Universidad Nacional de Colombia, sede Medellín, Colombia
[d] Traumatología y Ortopedia, Hospital Interzonal General de Agudos "Oscar Alende", Mar del Plata, Argentina

ARTICLE INFO

Article history:
Received 21 April 2010
Received in revised form 26 September 2010
Accepted 20 November 2010
Available online 25 December 2010

Keywords:
Bioactive coatings
Bone formation
Nanoindentation

ABSTRACT

Metals are the most widely used materials in orthopaedic and dental implants due to their excellent mechanical properties. However, they do not bond naturally with mineralized bone. Further, they can release metallic particles that may finally result in the removal of the implant. There are two strategies to avoid these drawbacks: one is to protect the metallic implant with a biocompatible coating and the other is to add bioactive particles to enhance implant fixation to the existing bone. In this work, surgical grade stainless steel implants coated with tetraethoxysilane (TEOS)–methyltriethoxysilane (MTES) and 10 wt.% of commercial wollastonite particles were implanted in the Hokkaido femur rats. Transversal sections of the tibia samples were examined with SEM, AFM, histological analysis and nanoindentation experiments in air and under physiological conditions to characterize the hydroxyapatite deposits and the composition of the newly formed tissue around the implant. The results showed no presence of harmful ions or metallic particles in the surrounding tissues and that the coating promoted formation and growth of new bone in the periphery of the implant, both in contact with the old bone (remodellation zone) and the marrow (new bone). The relative mechanical behavior of old, remodeled and new bone tissues obtained in air cannot be directly extrapolated to *live* or *in vivo-physiological* response. This may be caused by the different degree of hydration and SBF/structure interaction among the three types of bones but these values are near the normal hydrated bone response.

1. Introduction

The most common reasons for failure of orthopaedic or dental implants are biological incompatibility and/or degradation of the implant. Metals have excellent mechanical performance [1–3] and are widely used in orthopaedic surgery. However, the release of metallic particles due to wear or chemical degradation causing different pathologies may ultimately require the removal of the implant [4,5]. Besides, most metals cannot form a natural bond with mineralized bone. One effective way to diminish the ion release is by coating the metallic implant with a protective layer [5,6]. These films can be bioactive or can be functionalized with the addition of "bone-growth-inducing" particles [7–10]. Therefore, the coating acts as a barrier deterring the release of metal ions and it enables bonding with the old bone by the formation of hydroxyapatite.

Many coatings are used to improve the performance of metallic prosthesis. For example, biocompatibility can be improved with silica based on silane precursors [11,12]. Films obtained by the sol–gel technique have been successfully deposited on stainless steel, silver and aluminium, and they have been proven to enhance the oxidation and corrosion resistances of these metals [9,13]. It is possible to replace some inorganic components by organic ones which increase the viscoelastic deformation of the structure [14–16] thus leading to better adaptability to the substrate surface. Further, these systems have the possibility of having added particles to the coatings and be reinforced [17,18]. The addition of bioactive particles as well as dissolution and re-deposition of inorganic compounds of the apatite family have been studied [19–22] as an attempt to provide the basic metal bone-like formation and adhesion to the existing bone. Also, the mechanical properties of these coated systems are of great importance, since the system of implant/coating/existing bone is mechanically loaded as a unique component, so that their elastic and viscoelastic properties should be studied [17,23,24]. The nanomechanical properties of bone have

* Corresponding author. Juan B. Justo 4302, B7608FDQ. Mar del Plata, Argentina. Tel.: +54 223 481 6600; fax: +54 223 4810046.
E-mail address: jballarre@fi.mdp.edu.ar (J. Ballarre).

0928-4931/$ – see front matter © 2010 Elsevier B.V. All rights reserved.
doi:10.1016/j.msec.2010.11.030

been studied by several researchers in order to improve our knowledge of bone growth and regeneration in illness and heath [25–27].

In particular, titanium implants coated with plasma sprayed wollastonite [28–30] or filled with wollastonite in powder form [31] have been proven to have *in vitro* hydroxyapatite deposition ability, bone compatibility, osseo-conductivity and also bone inductivity in contact with the bone marrow.

In the present work we study implants made of stainless steel, which is a low-cost massively used material in orthopaedics. The main aim is to find out whether wollastonite particles have the ability to functionalize a protective coating applied by the sol–gel technique on stainless steel. The sol–gel method has been proposed as an appropriate procedure to process protective and bioactive coatings. The advantages and technological significance of sol–gel coatings over other coating methods have been widely demonstrated [32,33]. The coating produced in this work is an organic–inorganic one (called "hybrid") which was fabricated by the hydrolysis and polycondensation of a mixture formed by a purely inorganic compound, such as tetraethylorthosilane (TEOS), and an organic compound like methyltriethoxy-silane (MTES) together with the addition of wollastonite particles.

From a structural viewpoint, not only are the mechanical properties of the implant of main importance, but also is the quality of the regenerated bone [34,35]. Depth-sensing indentation has shown to be the most adequate technique to evaluate the mechanical properties of bones, especially when localized zones need to be studied [26]. Hence, depth-sensing indentation complemented with elemental analysis and imaging techniques have been used to study the mechanical behavior of the regenerated bone on the abovementioned coatings.

2. Experimental details

2.1. Materials

Stainless steel AISI 316L (Atlantic Stainless Co. Inc., Massachusetts, USA) in the form of wires (1.5 mm diameter and 2 cm length) and plates ($3\times2\times0.2$ cm^3) were used as substrates. The wires and plates were degreased, washed with distilled water and rinsed in ethanol before coating.

Hybrid organic–inorganic sols were prepared by acid catalysis using silicon precursors: tetraethylorthosilane (TEOS, 99%, ABCR GmbH & Co, Germany) and methyltriethoxy-silane (MTES, 98%, ABCR GmbH & Co, Germany) with absolute ethanol as solvent. The molar ratio of the silanes was maintained constant (TEOS/MTES = 40/60), and nitric acid (0.1 mol/L) was used as the catalyser which was formulated in our previous studies [22,36]. The sol was prepared by constant stirring at 40 °C for 3 h to obtain a final pH between 1 and 2 [37]. The final silica concentration for the sols was 3 mol/L. The amount of water was stoichiometrically maintained. The resulting sols were transparent with water-like viscosity.

The particle suspensions were prepared by adding 10 wt.% of commercial wollastonite particles (NYAD 1250, Minera NYCO SA, USA) with a medium diameter size of 3.5 μm to the TEOS–MTES sol. After adding 3 wt.% of phosphate ester surfactant [38] the suspensions were stirred applying high shear mixing in a rotor–stator agitator (Silverson L2R, UK) for 4 min.

A double-layer coating system was applied in two steps by dipping. The first layer prepared with TEOS–MTES sol was obtained at room temperature by dip-coating at a withdrawal rate of 4 cm min^{-1}, dried at room temperature for 0.5 h, and then heat treated for 0.5 h at 450 °C in an electric furnace. The second layer of TEOS–MTES with 10 wt.% wollastonite particles was applied on top of the first layer using the same withdrawal rate and thermal treatment for the coatings without the particles. Single coatings either with TEOS–MTES sol or TEOS–MTES with 10 wt.% wollastonite particles were also obtained by dipping and heat treated for 0.5 h at 450 °C to measure the film thickness by digital holographic microscopy.

2.2. In vitro analysis

Coated plates were tested by immersion for 60 days in simulated body fluid solution (SBF), which contained the amount of inorganic ions present in the human plasma [39]. The surface area/solution volume ratio was equal to 0.3 cm^2/mL. The solution was prepared and stored for a maximum of 30 days at 5 °C. The SBF for the immersion tests was exchanged every 8 days to avoid precipitation. The samples were retrieved at different periods of time. After the immersion, they were rinsed with distilled water and dried in air. The surfaces were observed using a scanning electronic microscope (SEM), Jeol JSM-5910 V.

2.3. In vivo experiments

2.3.1. Surgical implantation

In vivo experiments were conducted in total on 4 Hokkaido adult rats (weighted 350 ± 50 g) according to the codes and rules of the Ethics Committee of the National University of Mar del Plata (Interdisciplinary Committee, April 2005) and taking care of surgical procedures, pain control, standards of living and appropriated death. The application of the 3Rs (replace, reduce, refine) was attended to. Coated wires were sterilized in an autoclave for 20 min at 121 °C. Rats were anaesthetized with fentanyl citrate and droperidol (Janssen-Cilag Lab, Johnson and Johnson, Madrid, Spain) according to their weight. The region of the surgery surface was cleaned with antiseptic soap. The animals were placed in a supine position and the implantation site was exposed through the superior part of the femur's internal face. A region of, approximately, 0.5 cm in diameter was scraped in the femur plateau and a hole was drilled using a hand drill with a 1.5 mm diameter at a low speed. The implantation site was irrigated with physiological saline solution during the drilling procedure for cleaning and cooling purposes. The coated implants were placed by press fit into the femur, extending them into the medullar canal. The animals were sacrificed with an overdose of intraperitoneal fentanyl citrate and droperidol. After 60 days the bones with implants were abladed. Conventional X-ray radiographs were taken before retrieving the samples for control purposes.

2.3.2. Samples sectioning

The retrieved samples were cleaned from the surrounding soft tissues and fixed in neutral 10 wt.% formaldehyde for 24 h. Then, they were dehydrated in a series of acetone–water mixture followed by a methacrylated solution and, finally, embedded in methyl methacrylate (PMMA) solution and polymerized. The PMMA embedded blocks were cut with a low speed diamond blade saw (Buehler GmbH) cooled with water. Various sections were prepared for different experiments: sections of 200 μm in thickness for histological staining, AFM and SEM images, and blocks of 5 mm in thickness for nanoindentation studies. The nanoindentation samples were successively polished with 120, 240, 400 and 600 grit papers lubricated with water. The finest polishing was performed with a suspension of 3 μm alumina powder.

2.3.3. SEM, AFM and histological analysis

The surface morphology of the implant/bone interface was observed with scanning electron microscopy (SEM Jeol JSM-6460LV) under high vacuum with a detector operated at 15 kV. The samples were coated with a thin layer of gold. Elemental analysis was performed in the new bone zone formed between the implant and the marrow with an Energy-dispersive X-ray spectroscopy microanalyzer (EDAX Genesis XM4–Sys 60). The data recorded with the EDAX were analyzed using an EDAX Genesis (version 5.11) software. Also, Atomic Force Microscopy (AFM, Agilent 5500) superficial and topographic images were obtained for the old bone/new bone zone interface.

To observe the soft tissue and the bone lining cells, histological sections were stained with toluidine blue stain solution. The stained sample sections were observed using optical light microscopy (Olympus, BH2).

2.3.4. Nanoindentation measurements

Indentation measurements were performed using a fully calibrated UMIS-2000 (CSIRO, Australia) nanoindenter. This equipment has a displacement resolution 0.1 nm, internal noise uncertainty <0.1 nm, force resolution 0.75 μN and stage registration repeatability 0.2 μm. Load and depth were recorded simultaneously for complete load–unload cycles using a Berkovich indenter. The contact force for detection of the surface position was 0.15 mN. The loading and unloading rates were 1 mN/s. The maximum load was 10 mN and it was held constant for 30 s to avoid creep effects on the determination of the reduced modulus and to study the time-dependent response of the samples. Grids of 5×5 indentations separated by a distance of 10 μm were performed on each specimen in 3 locations: between the old bone and the implant (remodellation bone zone), between the marrow and the implant (new bone zone) and away from the implant (old cortex bone). It should be pointed out that the remodelled bone is newly formed bone after the implantation of the prosthesis. However, to differentiate it from the new bone deposited on the implant (which we denote as "new bone" in this paper), it will be called "remodellation bone" hereafter.

The first set of indentations was carried out at room temperature and 50% relative humidity. Then, the same specimens were tested under submerged conditions in physiological solution, after an immersion of 24 h. The final set of tests was also conducted under submerged conditions, after 7 days of immersion in the same physiological solution. The physiological solution used was a simulated body fluid (SBF) which was prepared according to a chemical composition similar to the human plasma [39] with a pH of 7.35 ± 0.05.

The contact stiffness (S) was calculated as the slope of the unloading curve between 20 and 95% of the maximum load, P_{max}. The hardness (H) and reduced modulus (E_r) were then evaluated from the unloading contact stiffness and the indenter contact area (A_c) based on the Oliver–Pharr theory [40,41] as:

$$E_r = \frac{S}{2}\sqrt{\frac{\pi}{A_c}} \tag{1}$$

$$H = \frac{P_{max}}{A_c} \tag{2}$$

with

$$A_c = 24.5h_c^2 \tag{3}$$

where the contact depth h_c is calculated from the displacement at maximum load (h_{max}) as:

$$h_c = h_{max} - 0.75\frac{P_{max}}{S}. \tag{4}$$

The values of reduced modulus and hardness are reported as mean ± std dev. The statistical significance between the new and remodellation bone zones was performed by the t-test using SigmaStat (SYSTAT Software Inc, Chicago, USA) with a significance threshold of $p<0.05$.

The error propagation for the plasticity index (E_r/H) is calculated as follows:

$$\Delta\left(\frac{E_r}{H}\right) = \left[\frac{\Delta E_r}{H} - \frac{E_r}{H^2}\Delta H\right] \tag{5}$$

3. Results and discussion

3.1. Morphological analysis

The average single-layer coating thickness for neat TEOS–MTES and TEOS–MTES with wollastonite particles was 0.50 ± 0.05 μm and 1.10 ± 0.10 μm, respectively. The surface coating composition is mostly based on amorphous SiO_2 which belongs to the TEOS–MTES, having wollastonite particles homogeneously distributed in the film. According to optical microscopic inspections, the coatings displayed good and smooth surface appearance, without flaws or cracks on the surface or around the wollastonite particles.

In the *in vitro* results, an apatite-like layer was formed on the surface of the TEOS–MTES–wollastonite coatings after immersion in SBF. The energy-dispersive X-ray spectroscopy essays showed Ca and P presence. Other elements, such as Na and Mg, are present as residues of the SBF, while Si is one of the elements composing the coatings. After 5 days of immersion, some Ca–P rich phase was formed on and around the wollastonite particles as they are the source of calcium required for the formation reaction [37]. EDAX measurements confirm that this new phase is mainly composed of Ca and P (Fig. 1). After 33 days of immersion, solid and homogeneous agglomerated spots of this Ca/P rich compound appeared (Fig. 2) due to the ionic exchange between the physiological solution and the coating, which provided Ca and P enrichment of the deposited phase, hence enhancing the solidification [42].

EDAX analysis was performed near the interface of the new bone zone and the coating as a way to determine if any harmful ions were released from the surface of the metal implant to the surrounding environment (Fig. 3). The elemental analysis did not show any presence of iron or nickel for the studied period of time (60 days). The particle release at longer times was not studied since we follow the 3 R's concept and, for the main purpose of this work, it is not acceptable to use a greater number of animals. The particle release was also analyzed in similar coatings for different periods of time by ICP techniques [43]. Furthermore, the relative concentration of calcium and phosphorous in the newly formed tissue was similar to bone, giving a Ca/P ratio of 1.59, compared to 1.67 found in stoichiometric hydroxyapatite (HAp) and 1.62 in cortical femur bone of rats [44].

Fig. 4 shows SEM images of the transversal section of the rat femur with the stainless steel coated bioactive implant after 60 days of implantation. Newly grown bone tissue is clearly identified around the implant. The inner image in the right bottom corner in Fig. 4 shows the region of the implant that is in contact with the old cortex

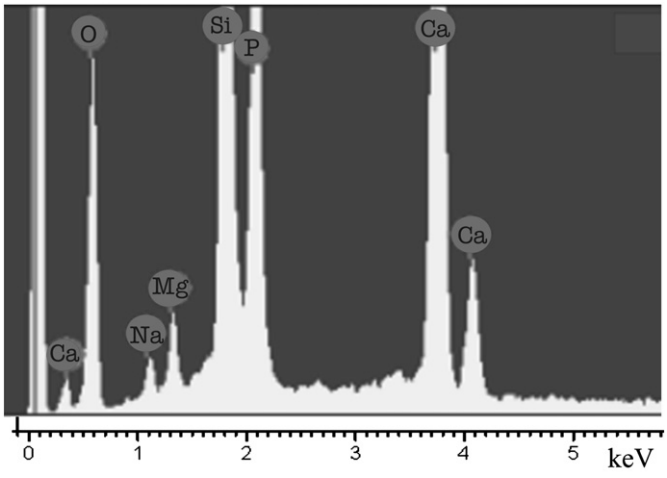

Fig. 1. EDAX analysis of the deposits over the TEOS–MTES with 10 wt.% wollastonite particles coating after 5 days of immersion in the simulated body fluid (SBF).

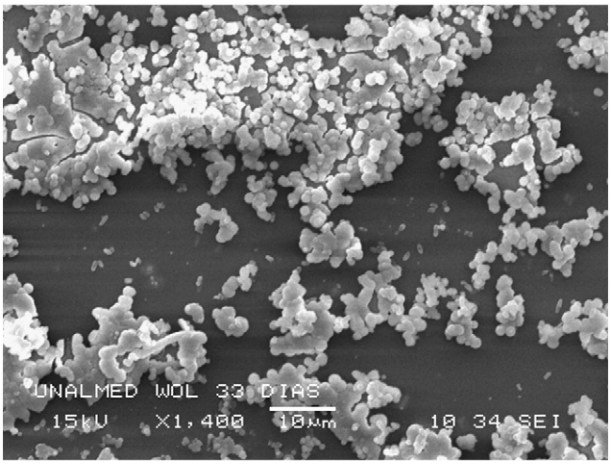

Fig. 2. SEM image of TEOS–MTES with 10 wt.% wollastonite particles coating after 33 days of immersion in the simulated body fluid (SBF), showing the presence of a Ca–P rich compound.

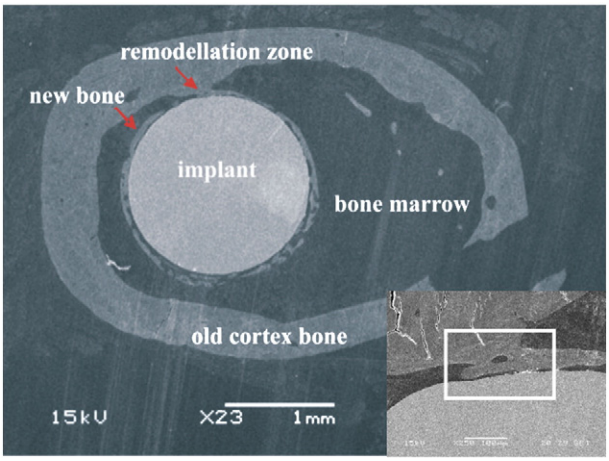

Fig. 4. SEM image for an overview cross-section of the TEOS–MTES–wollastonite coating after 60 days of implantation. Right bottom corner showing detail of the zone where the implant is in contact with the old cortex bone.

bone, while Fig. 5 shows a region of the implant surface in contact with the bone marrow.

There has been bone growth in the narrowest gaps between the old cortex and the implant as well as bone regeneration around the implant. This shows that the coating is fixed to the existing tissue and that it generates newly formed bone in its periphery. However, it can be seen that bone tissue is only partially attached to the implant, as is expected at the early stages of bone regeneration.

The remodellation zone (that is, the implant in contact with the old bone cortex) was examined using AFM as shown in Fig. 6. The old cortex and the remodelled bones are divided by a continuous groove of 0.33 ± 0.08 µm deep. The topography of these two regions differs in roughness, showing values of R_a of 0.025 µm for the old bone and 0.082 µm for the remodelled bone on a 100 μm^2 analyzed area. The inferior surface texture of the remodelled bone upon polishing reveals its less organized structure and perhaps lower mechanical properties and higher brittleness compared to the old bone [45].

3.2. Histological staining analysis

The histological images (Fig. 7) stained with toluidine blue tinge show that the position of the implant was placed in the femur bone (black zone) and the new bone tissue (in light pink and purple color) deposited over the bioactive hybrid wollastonite functionalized coating is clearly identified around the implant. Fig. 7(a) shows the tissue formed in contact with the bone marrow. This tissue is not fibrous and presents some vascularity and cell proliferation. The image also shows the old cortex tissue in the right corner of the image and a tissue bone connection between the implant and the cortex. The old cortex tissue can be distinguished from the new bone by its morphology and laminar structure. After 60 days of implantation the newly formed bone around the coated metal is not completely mature, presenting osteocytes and some osteocyte lacunae. However, it also has a laminar structure with osteoblasts at the growth interface. A stronger stain was done to certainly see the lining cells in the gap between the newly-formed tissue and the implant (Fig. 7 (b)). The bone formation surrounding the implant shows that TEOS–MTES–wollastonite coating not only promotes bone compatibility and osteoconductivity, but also displays bone inductivity in contact with the bone marrow environment.

3.3. Nanomechanical properties

In a previous work [24], the nanomechanical properties of the TEOS–MTES coatings have been studied, showing values of reduced modulus of 6.5 ± 0.3 GPa and 212 GPa for the stainless steel. The mean values of elastic modulus for trabecular and cortical bone in dry conditions [46] are 24.0 ± 2.3 GPa and 20.5 ± 2.3 GPa, respectively,

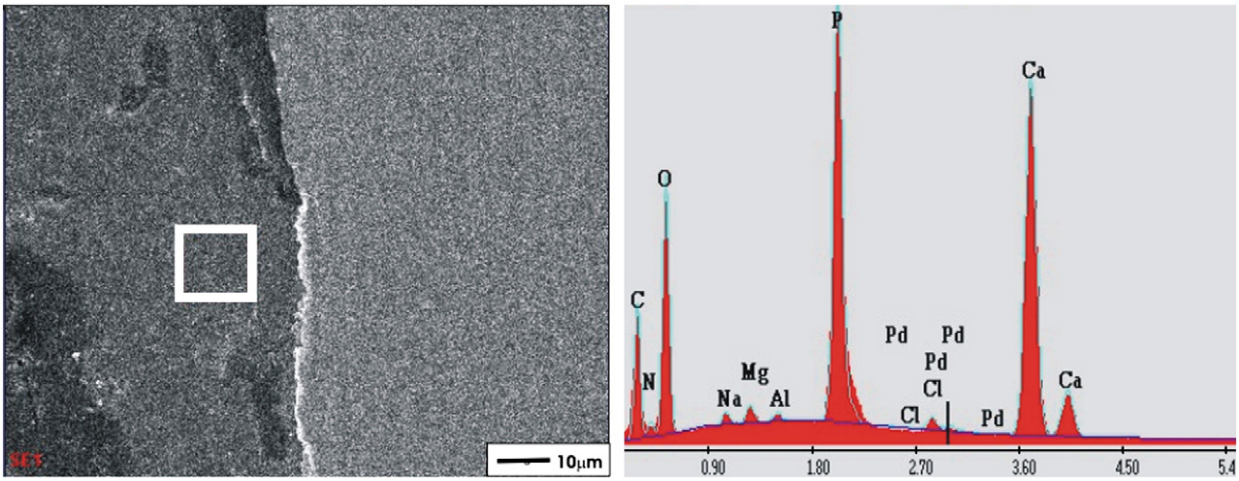

Fig. 3. Elemental EDAX analysis performed in a zone near the interface between the newly formed bone and the TEOS–MTES–wollastonite coating (delimited with a white box in (a)) after 60 days of implantation.

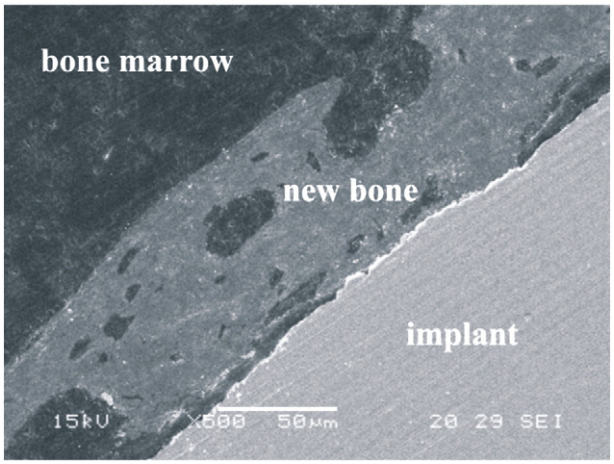

Fig. 5. SEM image of a region of the TEOS–MTES–wollastonite coated implant surface in contact with the bone marrow after 60 days of implantation.

indicating the importance in having a coating with elastic reduced modulus similar to the existing bone to avoid elastic mismatch.

Fig. 8 shows typical load–displacement nanoindentation curves of the three different bone tissues [(a) cortex bone, (b) new bone zone and (c) remodellation zone] in air and under submerged conditions in the simulated body fluid. The maximum indentation depth achieved at 10 mN is the highest in the submerged samples, illustrating the softening effect of the body fluid on old, remodelled and newly formed bone tissues.

The reduced modulus and the ratio E_r/H of the tested samples are presented in Figs. 9 and 10, respectively. The ratio E_r/H is usually referred to as the *plasticity or ductility index*, which reflects the relative amount of plastic indentation work [47]. It has also been shown to correlate well with the fracture toughness of the indented material [48], an important parameter in bone structural integrity.

The standard deviation is between 16 and 42% for E_r and 1 to 28% for the plasticity index for all samples. This is due to the inherent heterogeneity of the bone and the indentation size, which is in the order of the bone microstructures [26,49–52].

The new bone and remodellation zones yield similar mechanical behaviors. Compared to the old cortex bone tested in air, the new and remodellation bone tissues are less stiff and display marginally higher ductility indices.

Immersion in SBF deteriorates the stiffness and slightly increases the ductility of the old cortex bone. However, in the new bone, both stiffness and ductility are reduced. The effect of hydration (on samples immersed for 7 days in SBF) on stiffness and ductility is proportionally larger in the newly formed tissues (both new and remodellation bones) where the difference is −30% and −18% in the regenerated bone against −15% and +13% in the cortex bone. This occurs because the newly formed bone has higher percentage of absorbent/hydrophilic organic materials compared to the old cortex bone. In general, the reduced modulus and

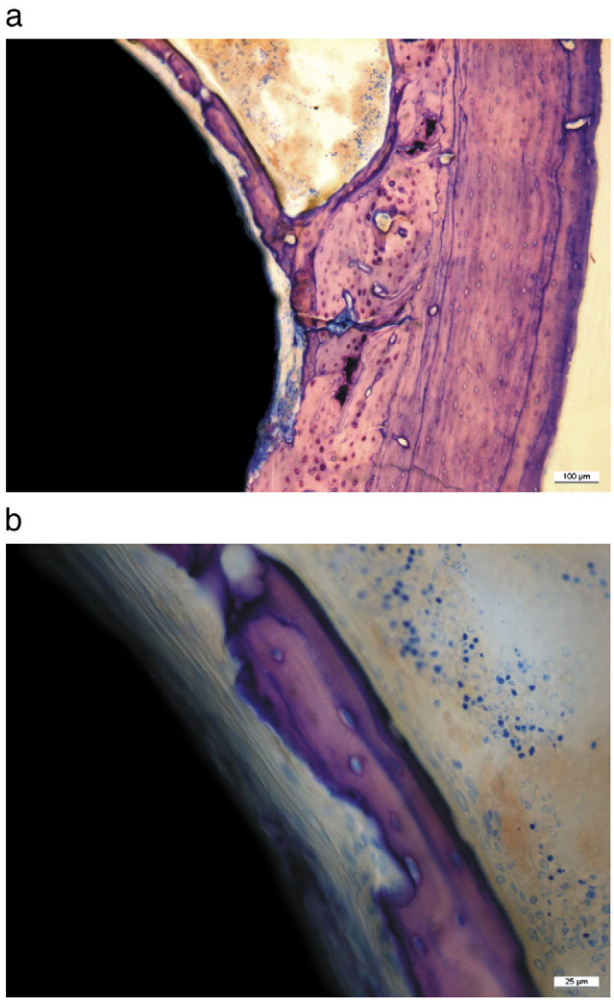

Fig. 7. Optical microscopic images of toluidine blue stained histology sections showing the implant, the remodellation and the newly formed bone (a). Detail of the presence of lining osteoblastic cells between the newly-formed bone and the coated implant (b).

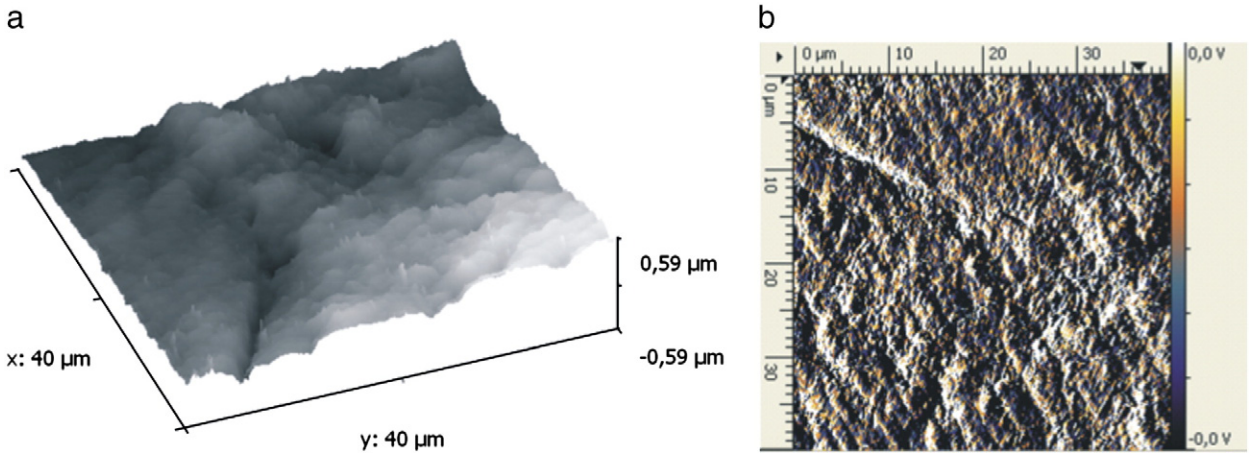

Fig. 6. AFM image of the remodellation bone zone and cortex bone. Both regions are divided by a continuous groove.

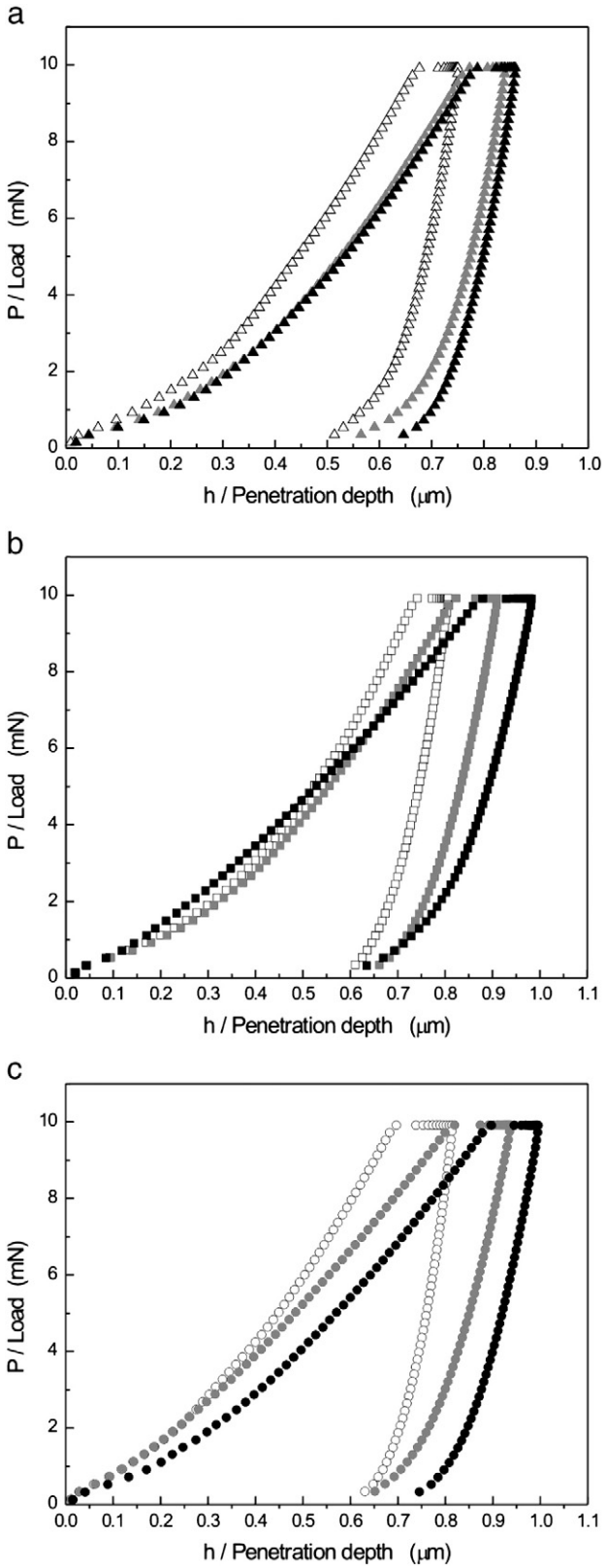

Fig. 8. Load–displacement curves with 10 mN maximum load of (a) old cortex bone (tested in: (Δ) air, (▲) with 1 day and (▲) 7 days of immersion), (b) new bone zone (tested in: (□) air, (■) with 1 day and (■) 7 days of immersion), and (c) remodellation bone zone (tested in: (○) air, (●) with 1 day and (●) 7 days of immersion).

ductility index decrease steadily with the submersion time. This indicates that the bones (old, remodelled and new bones) are not saturated after one day of immersion in SBF.

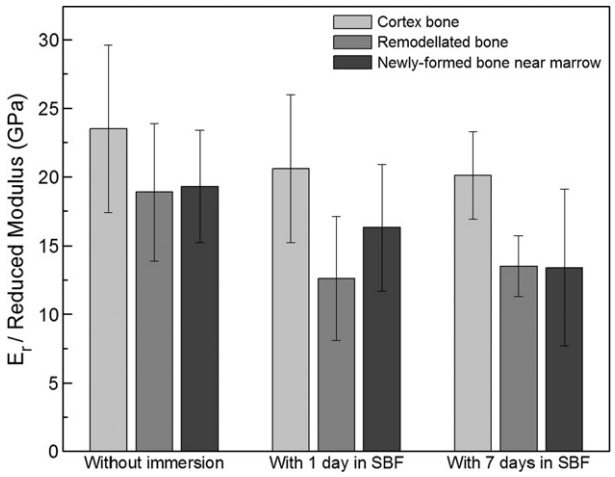

Fig. 9. Reduced moduli of three different types (old cortex, remodelled and newly-formed) of bone tissues tested in air, and submerged in SBF for 1 and 7 days.

The creep behavior in a load-step indentation test is characterized by the h/h_0 versus t curve [53], where h_0 is the initial displacement at maximum load and t is time. The average plus one standard deviation of creep values are shown in the curves in Fig. 11 for the three types of bone structures and immersion times studied. Creep increases with water content in the old cortex bone while it decreases in the new bone and shows no definite trend in the remodellation bone. This occurs because indentation creep is a mixture of plastic, viscoelastic and viscoplastic responses of the material [42]. Liquid absorption accentuates the mechanical time-dependency of solid materials due to liquid viscous response. However, plasticity is not always increased by liquids as seen in Fig. 10. As a result, it is obtained that a trend in creep behavior mostly follows that of the ductility index.

Note that the reduced modulus, ductility index and creep responses vary with immersion time, indicating that saturation is not reached at least after 1 day of immersion.

The indentation behavior of newly formed bone structures (that is, zones of new and remodellation bones) hydrated and tested in SBF has a close resemblance to that obtained on *ex-vivo* or non-calcified samples (in order to avoid deterioration of the collagen matrix) compared to the conventional decalcified methacrylate-embedded samples tested in air [46,54]. This proves the adequacy of this technique to analyse regeneration, fixation and healing of bone/implant interfaces.

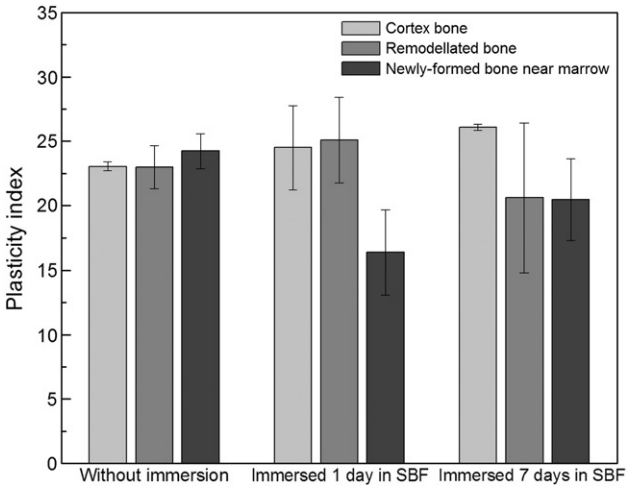

Fig. 10. Plasticity or ductility index E_r/H of three different types (old cortex, remodelled and newly-formed) of bone tissues tested in air, and submerged in SBF for 1 and 7 days.

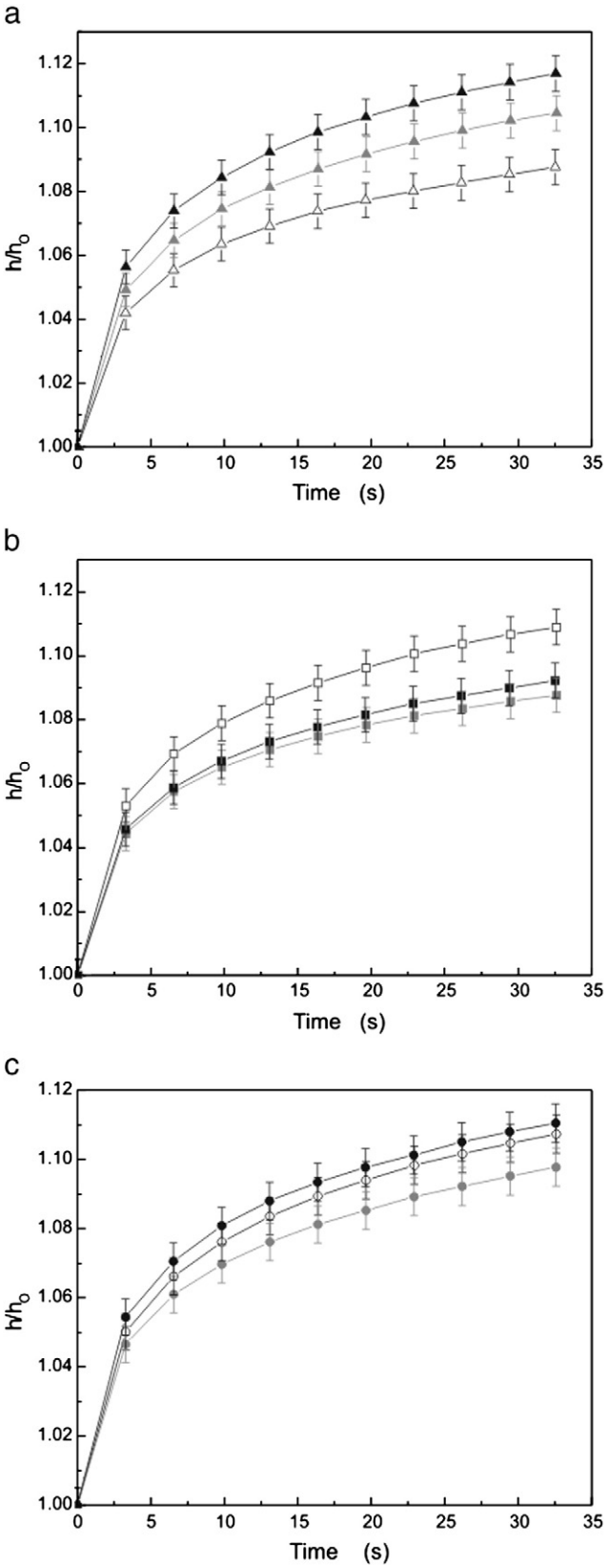

Fig. 11. Creep behavior of all bone samples under an applied load of 10 mN: (a) old cortex tested in: (Δ) air, (▲) with 1 day and (▲) 7 days of immersion; (b) new bone zone tested in: (□) air, (■) with 1 day and (■) 7 days of immersion, and (c) remodellation bone zone tested in: (○) air, (●) with 1 day and (●) 7 days of immersion.

Summarizing the nanoindentation results in Figs. 9–11, it is obvious that SBF hydration affects the mechanical behavior of pre-existent and regenerated bone tissues in different ways. That is, the stiffness decrement is higher in the latter; and the ductility index also decreases in the latter but increases in the former. Also, the creep resistance in SBF is reduced for the old cortex bone but is improved in the remodeled tissue. This indicates that the relative mechanical behavior of old, remodelled and newly formed bone tissues obtained in air cannot be directly extrapolated to *live* or *in vivo-physiological* response. This may be due to the different degree of hydration and SBF/structure interaction amongst the three types of bones.

5. Conclusions

It has been demonstrated that the bioactive sol–gel/wollastonite coating on surgical grade stainless steel promotes formation and growth of a new bone in the periphery of the implant, both in contact with the old bone (remodellation zone) and the marrow.

Nanoindentation studies under physiological conditions showed that the bone formation surrounding the implant has a good quasistatic and time-dependent nanomechanical behavior, comparable to the remodelled bone formed on the cortex. However, these two types of newly formed bone have lower modulus and are more brittle than the pre-existent (old) bone at this early stage of bone regeneration.

The mechanical parameters of old, remodelled and new bone tissues obtained in air are different to those obtained under physiological conditions, both absolute and relative values. This signifies the importance of testing the specimens submerged in SBF to adequately simulate their *live* or *in vivo* mechanical response.

It is also suggested that to obtain nanomechanical properties via nanoindentation tests on the bone under *saturated* physiological conditions, samples should be immersed for more than 7 days before testing.

Acknowledgments

The authors would like to acknowledge the financial supports from the following agencies: (a) DuPont-CONICET award, (b) Robust Equipment Projects of the National, (c) University of Colombia, and (d) the Australian Research Council.

References

[1] P.F. Doorn, P.A. Campbell, J. Worrall, P.D. Benya, H.A. MacKellop, H.C. Amstutz, J. Biomed. Mater. Res. 42 (1998) 103.
[2] K.S. Katti, Colloids Surf., B 39 (2004) 133.
[3] J.V. Sloten, L. Labey, R.V. Audekercke, G.V.D. Perre, Biomaterials 19 (1998) 1455.
[4] J.J. Bullen, H.J. Rogers, P.B. Spalding, C.G. Ward, FEMS Immunol. Med. Microbiol. 43 (2005) 325.
[5] Y. Okazaki, E. Gotoh, T. Manabe, K. Kobayashi, Biomaterials 25 (2004) 5913.
[6] J.A. Disegi, L. Eschbach, Int. J. Care Injured 31 (2000) 2.
[7] D.B. McGregor, R.A. Baan, C. Partensky, J.M. Rice, J.D. Wilbourn, Eur. J. Cancer 36 (2000) 307.
[8] D.A. López, A. Duran, S. Ceré, J. Mater. Sci. Mater. Med. 19 (2008) 2137.
[9] O. de Sanctis, L. Gomez, N. Pellegri, C. Parodi, A. Marajofsky, A. Duran, J. Non-Cryst. Solids 121 (1990) 338.
[10] J.J. de Damborenea, N. Pellegri, O. de Sanctis, A. Duran, J. Sol–Gel. Sci. Technol. 4 (1995) 239.
[11] A. Kros, M. Gerritsen, V.S.I. Sprakel, N.A.J.M. Sommerdijk, J.A. Jansen, R.J.M. Nolte, Sens. Actuators, B 81 (2001) 68.
[12] T. Chou, C. Chandrasekaran, G.Z. Cao, J. Sol–Gel. Sci. Technol. 26 (2003) 321.
[13] O. de Sanctis, L. Gómez, N. Pellegri, A. Durán, Surf. Coat. Technol. 70 (1995) 251.
[14] P. Galliano, J.J. de Damborenea, M.J. Pascual, A. Duran, J. Sol–Gel. Sci. Technol. 13 (1998) 723.
[15] L.E. Amato, D.A. López, P.G. Galliano, S.M. Ceré, Mater. Lett. 2005 (2005) 2026.
[16] D.A. López, N.C. Rosero-Navarro, J. Ballarre, A. Durán, M. Aparicio, S. Ceré, Surf. Coat. Technol. 202 (2008) 2194.
[17] J. Ballarre, E. Jimenez-Pique, M. Anglada, S. Pellice, A.L. Cavalieri, Surf. Coat. Technol. 203 (2009) 3325.
[18] J. Ballarre, S.A. Pellice, W.H. Schreiner, S. Ceré, Key Eng. Mater. 396–398 (2009) 311.

[19] P.N. De Aza, Z.B. Lucjlinska, C. Santos, F. Guitian, S. De Aza, Biomaterials 24 (2003) 1437.
[20] A. Oyane, K. Nakanishi, H.-M. Kim, F. Miyaji, T. Kokubo, N. Soga, T. Nakamura, Biomaterials 20 (1999) 79.
[21] O. Peitl, E.D. Zanotto, L.L. Hench, J. Non-Cryst. Solids 292 (2001) 115.
[22] J. Ballarre, D.A. López, W.H. Schreiner, A. Durán, S.M. Ceré, Appl. Surf. Sci. 253 (2007) 7260.
[23] J. Ballarre, D.A. López, A.L. Cavalieri, Wear 266 (2009) 1165.
[24] J. Ballarre, D.A. López, A.L. Cavalieri, Thin Solid Films 516 (2008) 1082.
[25] O. Brennan, O.D. Kennedy, T.C. Lee, S.M. Rackard, F.J. O'Brien, J. Biomech. 42 (2009) 498.
[26] G. Pelled, K. Tai, D. Sheyn, Y. Zilberman, S. Kumbar, L.S. Nair, C.T. Laurencin, D. Gazit, C. Ortiz, J. Biomech. 40 (2007) 399.
[27] J.-Y. Rho, T.Y. Tsui, G.M. Pharr, Biomaterials 18 (1997) 1325.
[28] W. Xue, X. Liu, X. Zheng, C. Ding, Biomaterials 26 (2005) 3455.
[29] X. Liu, C. Ding, Z. Wang, Biomaterials 22 (2001) 2007.
[30] X. Liu, C. Ding, Mater. Lett. 57 (2002) 652.
[31] N. Sahai, M. Anseau, Biomaterials 26 (2005) 5763.
[32] S. Sakka, J. Sol–Gel. Sci. Technol. 3 (1994) 69.
[33] M. Guglielmi, J. Sol–Gel. Sci. Technol. 8 (1997) 443.
[34] P. Fratzl, H.S. Gupta, E.P. Paschalis, P. Roschger, J. Mater. Chem. 14 (2004) 2115.
[35] P. Fratzl, R. Weinkamer, Prog. Mater. Sci. 52 (2007) 1263.
[36] J. Ballarre, J.C. Orellano, C. Bordenave, P. Galliano, S. Ceré, J. Non-Cryst. Solids 304 (2002) 278.
[37] C. Garcia, S.M. Ceré, A. Durán, J. Non-Cryst. Solids 348 (2004) 218.
[38] A.K. Maiti, B. Rajender, Mater. Sci. Eng., A 333 (2002) 35.
[39] T. Kokubo, H. Kushitani, S. Sakka, T. Kitsugi, T. Yamamuro, J. Biomed. Mater. Res. 24 (1990) 721.
[40] W.C. Oliver, G.M. Pharr, J. Mater. Res. 19 (2004) 3.
[41] W.C. Oliver, G.M. Pharr, J. Mater. Res. 7 (1992) 1564.
[42] Y. Zhang, M. Mizuno, M. Yanagisawa, H. Takadama, Mater. Res. Soc. 18 (2003) 433.
[43] A. Duran, A. Conde, A. Gómez Coedo, T. Dorado, C. García, S. Ceré, J. Mater. Chem. 14 (2004) 2282.
[44] P.M. Lind, C. Wejheden, R. Lundberg, P. Alvarez-Lloret, S.A.B. Hermsen, A.B. Rodriguez-Navarro, S. Larsson, A. Rannug, Chemosphere 75 (2009) 680.
[45] I.D. Marinescu, H.K. Tonshoff, I. Inasaki, Handbook of Ceramic Grinding and Polishing, William Andrew Publishing/Noyes, 2000.
[46] S. Hengsberger, A. Kulik, P. Zysset, Bone 30 (2002) 178.
[47] J.A. Greenwood, J.B.P. Williamson, Proc. R. Soc. London, Ser. A 295 (1966) 300.
[48] K. Tanaka, J. Mater. Sci. 22 (1987) 1501.
[49] J.A. Shibli, M. Feres, L.C. de Figueiredo, G. Iezzi, A. Piattelli, J. Contemp. Dent. Pract. 8 (2007) 1.
[50] M. Mastrogiacomo, S. Scaglione, R. Martinetti, L. Dolcini, F. Beltrame, R. Cancedda, R. Quarto, Biomaterials 27 (2006) 3230.
[51] L. Mulder, J.H. Koolstra, J.M.J. den Toonder, T.M.G.J. van Eijden, Bone 41 (2007) 256.
[52] W. Schneiders, A. Reinstorf, W. Pompe, R. Grass, A. Biewener, M. Holch, H. Zwipp, S. Rammelt, Bone 40 (2007) 1048.
[53] R. Seltzer, Y.-W. Mai, Eng. Fract. Mech. 75 (2008) 4852.
[54] P. Ammann, I. Badoud, S.B. Barraud, R. Dayer, R. Rizzoli, J. Bone Miner. Res. 22 (2007) 1419.